MULTISPECTRAL IMAGE PROCESSING FOR ENVIRONMENTAL MONITORING

Mark J. Carlotto
Mark B. Lazaroff
Mark W. Brennan

TASC
55 Walkers Brook Dr.
Reading MA 01867 (USA)

ABSTRACT

New techniques are described for detecting environmental anomalies and changes using multispectral imagery. Environmental anomalies are areas that do not exhibit normal signatures due to man-made activities and include phenomena such as effluent discharges, smoke plumes, stressed vegetation, and deforestation. A new region-based processing technique is described for detecting these phenomena using Landsat TM imagery. Another algorithm that can detect the appearance or disappearance of environmental phenomena is also described and an example illustrating its use in detecting urban changes using SPOT imagery is presented.

1. INTRODUCTION

Over the last twenty years a variety of techniques have been developed for monitoring different aspects of the environment using multispectral imagery (MSI). This paper describes two new techniques that have been developed to detect environmental anomalies and changes using commercial MSI data such as Landsat and SPOT. The techniques are of potential benefit in air pollution analysis, water quality assessment (point and non-point sources), the detection and remediation of hazardous waste sites, and other applications. Environmental anomalies are areas that do not exhibit normal signatures due to man-made activities. Phenomena such as effluent discharges, smoke plumes, and stressed vegetation are examples of environmental anomalies. A new technique is described for detecting these phenomena within a single image. A region-based approach is developed to enhance very subtle variations over the image in order to identify forest damage, water pollution, and smoke plumes in Landsat TM.

Change detection involves assessing differences in a scene over time by comparing two or more coregistered images. A new algorithm that can detect the appearance or disappearance of environmental phenomena is described. The algorithm adapts to global differences between images (i.e., selected MSI bands or features) on a region-by-region basis. An example illustrating its use in detecting urban changes in SPOT imagery is presented.

The organization of the paper is as follows: Section 2 describes a computational approach to environmental monitoring using MSI. Sections 3 and 4 summarize requisite algorithms for atmospheric correction, spectral feature extraction, and spectral classification. Section 5 and 6 detail the environmental anomaly and change detection algorithms. Examples from two study areas are presented in Section 7.

2. ENVIRONMENTAL MONITORING USING MSI

Fig. 1 is an overview of our approach to environmental monitoring using MSI. For examining surface phenomena we employ an atmospheric correction technique to remove smoke and haze from all bands. The corrected data are then converted into a set of features that describe physically-significant parameters of the surface such as the soil brightness, biomass/vegetation index, wetness, moisture stress index, vegetation temperature, and water quality (chlorophyll concentration, turbidity, and water temperature). The atmospheric component is estimated and processed in a slightly different way to assess atmospheric phenomena. Spectral classification is used to identify water, general vegetation, trees, built up areas, and other categories of interest. Spectral classification maps are used in conjunction with environmental feature sets to detect environmental anomalies and changes in those features over certain regions in the image.

0-8194-1020-9/93/$4.00

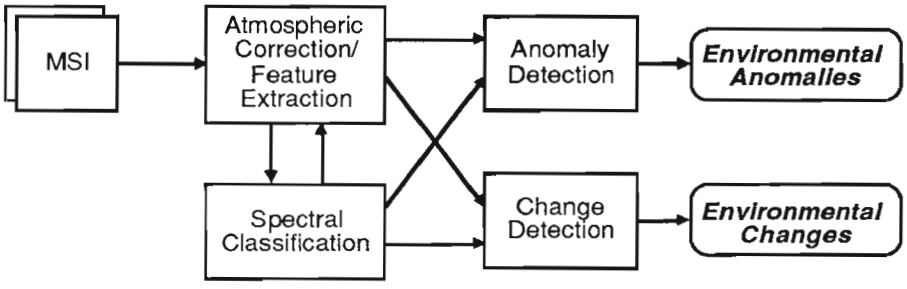

Fig. 1 Computational approach for environmental monitoring using MSI

3. ATMOSPHERIC CORRECTION/FEATURE EXTRACTION

Aerosols and particulates in the atmosphere can potentially affect our ability to detect environmental anomalies and changes in three ways: 1) by making it difficult to accurately and consistently classify surface categories, 2) by corrupting the computation of environmental features, and 3) by introducing non-significant differences between images. A de-hazing technique developed by Lavreau[1] is used to correct the imagery on a local basis. The method uses the fourth tasseled cap feature (see below) as an estimate of the haze and smoke component which is removed from six of seven Landsat TM bands.

Following atmospheric correction, spectral feature extraction is performed to reduce the data to a smaller number of bands or features in order to reduce computational complexity, and to transform the information into features that are physically meaningful. Table 1 is a partial list of MSI features that are useful for identifying surface and atmospheric features, and detecting environmental anomalies and changes. The first four provide measurements of soil brightness, biomass, moisture content, and atmospheric haze/smoke[2]. The normalized difference vegetation index (NDVI) and moisture stress index (MSVI) are used to assess the density and health of green vegetation[3,4]. The effect of illumination variations across the image is reduced by using the ratio of the band differences. A similar ratio of differences is used for MSVI as well. The relative temperature of vegetation, bodies of water, and atmospheric phenomena (e.g., to discriminate smoke from clouds) can be obtained from the thermal IR band. Measures of turbidity[5] and chlorophyll concentration[6] are used to evaluate water quality.

Feature	Formula
Brightness	$.3037\,B_1 + .2793\,B_2 + .4743\,B_3 + .5585\,B_4 + .5082\,B_5 + .1863\,B_7$
Greenness	$-.2848\,B_1 - .2435\,B_2 - .5436\,B_3 + .7243\,B_4 + .0840\,B_5 - .1800\,B_7$
Wetness	$.1509\,B_1 + .1973\,B_2 + .3279\,B_3 + .3406\,B_4 - .7112\,B_5 - .4572\,B_7$
TC4 (Atmospheric Component)	$.8461\,B_1 - .7031\,B_2 - .4640\,B_3 - .0032\,B_4 - .0492\,B_5 - .0119\,B_7$
Normalized Difference Vegetation Index (NDVI)	$\frac{B_4 - B_3}{B_4 + B_3}$
Moisture Stress Vegetation Index (MSVI)	$\frac{B_5 - B_4}{B_5 + B_4}$
Temperature	B_6
Turbidity	$\frac{B_3}{B_1}$
Chlorophyll-a	$.0106\,B_2^3 - .95912 \log B_5 + 6.40368\,\frac{B_3}{B_1} - 3.09667$

Table 1 MSI features for environmental monitoring

4. SPECTRAL CLASSIFICATION

Spectral classification is performed to identify specific areas in the image for anomaly and change detection. The classification of surface and atmospheric phenomena on the basis of spectral information is typically an interactive process involving image clustering/segmentation, supervised classification, and post-processing. Unsupervised techniques can be used to extract spectrally homogeneous regions but the process is usually highly compute-intensive. In most cases, the resultant regions must still be labeled by hand. Alternatively, knowledge-based techniques can be used to identify general categories based on spectral shape and/or relative brightness values in certain bands or features[7]. For Landsat TM the following rules are often applicable

- The spectrum of green vegetation is characterized by a peak in the near IR and can be classified by finding pixels where (band 4 > band 5) and (band 4 > band 3).
- Forested areas typically appear darker than other vegetation in the visible and can be separated from other vegetation by thresholding (band 2 < threshold)
- Water is very dark in the IR and can be extracted by thresholding, e.g., (band 4 < threshold)
- Soil-like materials (including built-up areas) have an increasing response in the IR (i.e., band 4 < band 5 < band 7) and have a relatively high brightness value

Similar strategies can be used to classify atmospheric phenomena as well; e.g.,

- Smoke can be extracted by thresholding pixels with large TC4 values, grouping the pixels into regions, computing the average temperature over each region, and selecting the warmest regions.
- Clouds like concrete and dry bare soil have high brightness values. Typically clouds are colder than concrete and bare soil and can be discriminated using the thermal IR band.

We apply the above techniques interactively to generate mask images for each spectral category of interest. As described below, these masks are used to average environmental features over regions of interest for anomaly detection, and to compute regional feature statistics for change detection.

5. ANOMALY DETECTION

Anomaly detection refers to the identification of those parts of an image that differ in some way from the rest of the image (the background). In the present context, environmental anomalies are defined to be those areas where the values of certain features are significantly different from the background. In some cases the anomalies are caused by man-made activities which may be observed directly in effluent discharges into adjacent water bodies, smoke plumes, or viewed over time as changes in the state of green vegetation, for example.

Environmental anomaly detection involves four steps: 1) selecting a portion of the scene for study, 2) computing the appropriate features over those regions, 3) thresholding the resultant features, and 4) combining and presenting the results. Spectral classification is performed to identify specific parts of the scene for study such as bodies of water, forested areas, atmospheric plumes, etc. Features such as NDVI, MSVI, and temperature can be used as the basis for detecting vegetation that has been damaged chemically or mechanically. Measures of turbidity and chlorophyll concentration along with temperature can be used to detect effluent discharges and assess relative differences in water quality. TC4 can be used to detect smoke and haze and temperature can be used to discriminate smoke from haze. Frequently the phenomena of interest are subtle and do not contribute to the formation of well-defined modes in the histogram (Fig. 2). Thresholding the feature will tend to produce a detection image that is highly speckled (Fig. 3).

These observations lead to a region-based formulation of the problem. In general, the performance of detection algorithms are limited by the signal-to-noise ratio (SNR) of the data; i.e., SNR limits the ability to detect subtle phenomena masked by the background. Spatial averaging can potentially improve SNR at the expense of decreased spatial resolution. In particular, if the pixels are drawn from the same population and are independent, averaging N pixels reduces the noise variance by a factor of 1/N and thus increases the SNR by a factor of $N^{1/2}$. Spatial averaging over a regular grid will not, in general, improve the SNR since it may average pixels from different populations. However, by averaging within connected regions of the same population (e.g., forested regions) the ability to detect very small differences between regions can be enhanced. Since forest damage, water pollution, deforestation, and other environmental phenomena often occur at larger spatial scales the tradeoff of resolution for increased SNR may be appropriate in many applications.

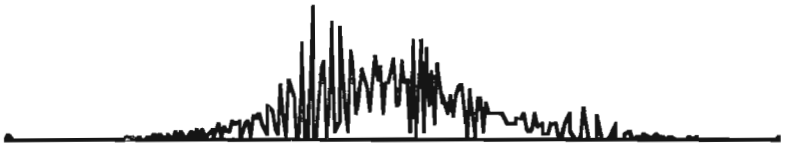

Fig. 2 Histogram of NDVI image over forest pixels

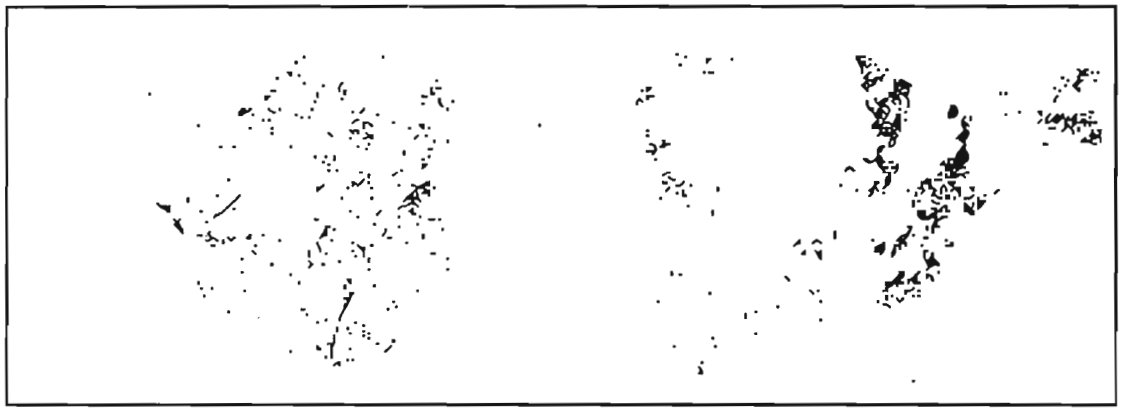

Fig. 3 Forest pixels with lowest NDVI (bottom 1%)

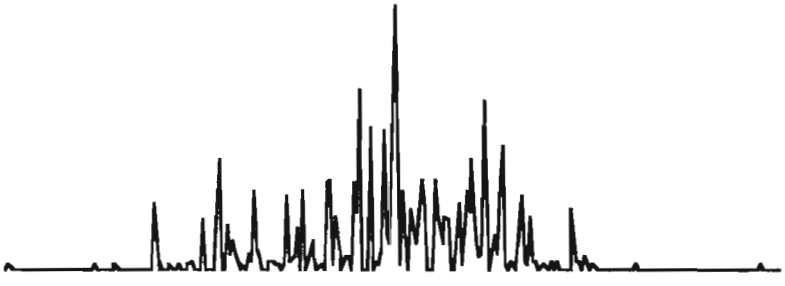

Fig. 4 Histogram of NDVI image over forest regions

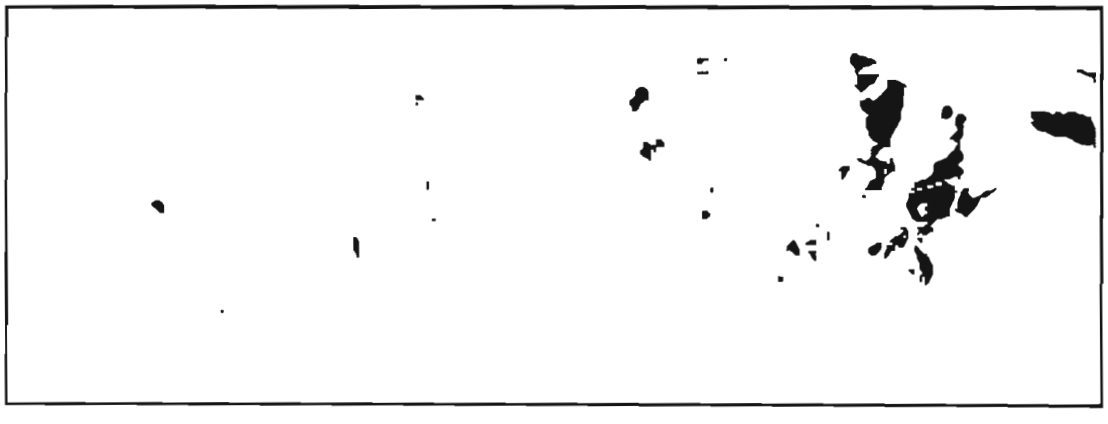

Fig. 5 Forest regions with lowest NDVI (bottom 1%)

To illustrate our region-based anomaly detection technique consider the following example. Figs. 2 and 3 show the histogram of an NDVI image computed over forested areas and the image obtained by thresholding the bottom 1% of the NDVI image. The black pixels are areas where the NDVI is relatively low and may be due to vegetation that is damaged. Fig. 4 shows the histogram of an NDVI image that has been smoothed over connected forest regions. A much richer mode structure is apparent. By thresholding that image by the same amount as before, we obtain a result (Fig. 5) which more clearly indicates those forest regions where the NDVI is significantly lower than average.

6. CHANGE DETECTION

In order to detect changes using multiple images acquired under different acquisition and environmental conditions, one must compensate for, or adapt to, non-significant (systematic) differences between the images. Previous algorithms[8,9] adapt to these differences on a local basis (i.e., within a sliding window) and can only detect changes whose size is comparable to that of the window.

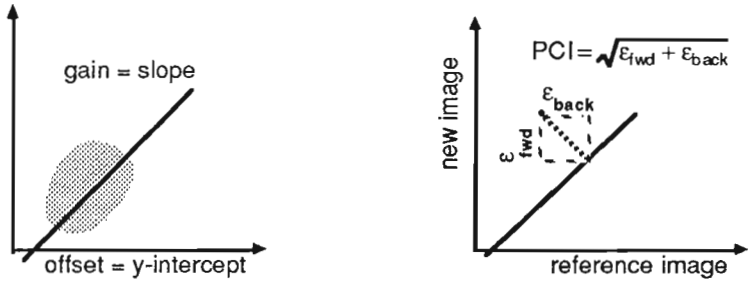

Fig. 6 Pixels in coregistered image correspond to points in joint distribution (left). Changes in imagery are deviations from the regression line. The perpendicular change index (PCI) is the distance from a point in the joint feature space to the regression line (right).

This section describes a new algorithm for detecting environmental changes using MSI. The algorithm is based on the concept of a perpendicular change index (PCI) which involves analyzing the joint distribution of pixel values from two coregistered images (selected MSI bands or features) taken at different times (Fig. 6). The analysis is performed on a region-by-region basis in order to adapt to any global differences between the two images. Regions can be defined either by a regular grid or be specific land cover categories extracted by spectral classification as described earlier. The data within a region is modelled by a linear relation

$$\mathbf{y} = \mathbf{M}\mathbf{x} + \mathbf{b}$$

where $\mathbf{x} = \{x_k\}$ are the feature values in the reference image, $\mathbf{y} = \{y_k\}$ are the feature values in the new image, $\mathbf{M}$ is a linear transformation, and $\mathbf{b}$ is a vector of constants. Typically the features are uncorrelated, so the model becomes:

$$y_k = m_k x_k + b_k$$

We define the forward prediction error to be the error in predicting the new image from the old image; i.e., $\mathbf{y}$ from $\mathbf{x}$:

$$\varepsilon_{forward} = \min_{\{m_k\},\{b_k\}} E\left[\sum_k (y_k - m_k x_k - b_k)^2\right]$$

where E denotes expectation. The coefficients which minimize the error are given by:

$$\frac{\partial \varepsilon_{forward}}{\partial m_k} = 0, \text{ and } \frac{\partial \varepsilon_{forward}}{\partial b_k} = 0$$

The backward prediction error is defined similarly:

$$\varepsilon_{\text{backward}} = \min_{\{n_k\},\{c_k\}} E\left[\sum_k (x_k - n_k y_k - c_k)^2\right]$$

where

$$x_k = n_k\, y_k + c_k$$

and the coefficients are found by least squares in a similar fashion. If the forward prediction error is substantially larger than backward error it is likely that the change was caused by the appearance of a structure which is significantly different from the background. Similarly if the backward prediction error is substantially larger than the forward error it is likely to be a disappearance. The total change in the image (Fig. 6) is given by

$$\text{PCI} = \sqrt{\varepsilon_{\text{forward}} + \varepsilon_{\text{backward}}}$$

and is the perpendicular distance from a point in the joint feature space to the regression line as shown in Fig. 6.

7. CASE STUDIES

This section shows how the preceding techniques can be used to detect smoke plumes, forest damage, and water pollution in central Europe, and urban change in the eastern U.S.

7.1 BITTERFELD, GERMANY

7.1.1 Background

Bitterfeld, in former East Germany has a high concentration of chemical manufacturing, mining and military training activities. Because of the high sulphur coal supply, strip mines are concentrated around Bitterfeld where dust storms scatter the coal dust into the atmosphere. With respect to air pollution, Bitterfeld ranks among the worst in the world[10], yielding one of the world's highest concentrations of sulphur dioxide. Additionally, chlorine gases, heavy concentrations of solvents, and hundreds of tons of hydrochloric acid are emitted into the atmosphere each year.

Vegetation damage has been documented as a result of wet sulfate precipitation (acid rain/soil acidification) and is aggravated by efficient deposition on forest canopies. Chemical manufacturing in Bitterfeld contributes to magnesium deficiency, heavy metal toxicity to roots, and moisture sensitivity which can lead to forest decline. Military training activities in the region create the potential for mechanical damage to the forest ecosystem.

Outdated, limited, or non-existent water pollution control devices and wastewater treatment capabilities in over 500 facilities contribute to severe water pollution problems in the area. Over 2400 substances that include toxic organics and heavy metals flow out of the plants as liquid waste into local streams, canals, and lakes (point sources). Discharges of untreated or poorly treated wastewater normally have high levels of biochemical oxygen demand, nutrients, and suspended solids. Potential non-point sources of water pollution caused by runoff of soil, nitrates, and pesticides are caused by agricultural activity in the region surrounding Bitterfeld as well.

7.1.2 Data

An area approximately 45 km by 24 km near Bitterfeld was selected for study. Fig. 7 shows a 1589x810 pixel image from a geocoded Landsat TM image acquired on September 4, 1986. Bitterfeld (near bottom center) is the source of a dense smoke plume (left). The Mulde River runs south-north through the middle of the image. Ground truth data consisting of field reports and photography were collected at 17 locations during a two day period in March 1992 to analyze our results. The following subsections describe experiments to detect smoke plumes, forest damage, and water pollution using this imagery.

7.1.3 Smoke Plumes

As noted earlier the fourth tasseled cap feature (TC4) has been shown to be a useful measure of atmospheric state for the purpose of removing the haze component in Landsat TM. To detect haze and smoke we threshold TC4 and select the pixels with the largest values (top 1%). The thresholded image is smoothed with a Gaussian filter (σ=10 pixels) to estimate the local density of smoke/haze pixels. The densest regions (top 5%) are thresholded and labeled. The thermal IR band is averaged over each region to assess the relative temperature of the region.

The TC4 feature computed over Bitterfeld is shown in Fig. 8 (top). The relative temperatures for 15 candidate regions are shown color-coded at the bottom. Regions with the largest thermal IR values were over the smoke plume originating from Bitterfeld and over a smaller plume to the north. Regions with lesser amounts of smoke or haze over water had lower values.

7.1.4 Forest Damage

Forest regions were extracted by spectral classification as outlined in Section 4. Forest pixels were further subdivided into evergreen and deciduous forests. Over each connected set of forest pixels the average NDVI, MSVI, and canopy temperature were computed. NDVI is an indicator of photosynthetic activity and plant vigor; MSVI measures moisture-related plant stress.

The region is dominated by evergreen forests. For evergreen forests there was a strong negative correlation between NDVI and temperature (-0.78), i.e., canopies emitting the greatest amount of thermal energy tend to have the lowest NDVI, and vice versa. No significant correlation was measured between NDVI and MSVI or MSVI and temperature (< 0.3). Fig. 9 shows the average MSVI over evergreen forests.

Only about 3% of the total forest area consists of deciduous trees. As above a strong negative correlation between NDVI and temperature (-0.83) was measured for deciduous forests. Stronger correlations between NDVI and MSVI (-0.76) and between MSVI and temperature (0.59) were also noted.

The greatest amount of forest damage appears to the north of Bitterfeld in a military training area as shown in Fig. 9. This area is near a small lake which was found to be chemically contaminated. Other damaged areas can be found east of Bitterfeld near a field of natural gas wells and west next to the main industrial area.

A second image was acquired a year later to check the consistency of these results. Overall, few changes in the vegetative state were found ($\rho \sim 0.77$ between NDVI values).

7.1.5 Water Pollution

Water bodies were also extracted by spectral classification as outlined in Section 4. For each body of water the average turbidity, chlorophyll concentration, and temperature were computed. Nephelometric turbidity units were used to assess the water quality. The chlorophyll concentration measures the bio-optical state of the water. Overall there was strong positive correlation among all three features (0.73-0.87).

Two water bodies were compared: a lake on the Mulde River (Big Lake) and Silver Lake. Both had roughly the same chlorophyll levels. Silver Lake was found to be significantly warmer[11] (Fig. 10) by about 6°F and significantly more turbid.

7.2 NORTHERN VIRGINIA

7.2.1 Background and Data

The second study area in northern Virginia is west of Washington D.C. Two SPOT panchromatic images one year apart in 1987 and 1988 were coregistered. A 1024 by 1024 pixel region was selected for study and is shown in Fig. 11. Dulles Airport is at the top of the photograph.

7.2.2 Change Detection Results

For this particular example multispectral information was not available to identify specific regions. Instead the image was divided into sub-blocks 256 by 256 pixels in size. Two change detection images were calculated. First the total change

(PCI) was computed within and averaged over each of the sub-blocks. This result shown in Fig. 11 identifies those regions with the greatest change and is particularly useful in viewing reduced resolution results from very large images. In Fig. 11 we also show the forward and backward prediction error images at full-resolution centered over the sub-block with the highest change. The disappearance of a linear structure (possibly a temporary road) and the appearance of several new buildings and other structures are noted.

9. CONCLUSION

New techniques for detecting environmental anomalies and changes using Landsat and SPOT imagery were introduced. A region-based anomaly detection technique was described and used to detect forest damage, water pollution, and smoke plumes. A new change detection algorithm that can detect the appearance or disappearance of environmental phenomena was also described and an example illustrating its use in detecting urban changes in SPOT imagery was presented.

We are continuing to assess and refine the methodology outlined in this paper. Further testing of the anomaly detection and change detection techniques is being performed on data sets over additional study areas.

8. REFERENCES

1. J. Lavreau, "De-hazing Landsat Thematic Mapper images," *Photogrammetric Engineering and Remote Sensing*, Vol. 57, No. 10, Oct 1991, pp 1297-1302.

2. R. Kauth and G. Thomas, "The tasseled cap: A graphic description of the spatio-temporal development of agricultural crops as seen by Landsat," in *Proceedings, 3rd Symposium on Machine Processing of Remotely Sensed Data*, Purdue University, 1976.

3. A. S. Hope, S. N. Goward, and D. E. Petzold, "Tersail: A numerical model for combined analysis of vegetation canopy bidirectional reflectance and thermal emissions," *Remote Sensing of Environment*, Vol. 26, pp 287-300, 1988.

4. B. N. Rock, T. Hoshizaki, J. R. Miller, "Remote detection of forest damage," *Bioscience*, Vol. 36, pp 439-445, 1986.

5. D. G. Brown and S. J. Walsh, "Compatibility of non-synchronous in-situ water quality data and remotely sensed spectral information for assessing lake turbidity levels in complex and inaccessible terrain," *Geocarto International*, Vol. 6, No. 2, pp. 5-12, 1991

6. C. A. E. Garcia and I. S. Robinson, "Chlorophyll-a mapping using airborne thematic mapper in Bristol Channel," *International Journal of Remote Sensing*, Vol. 12, No. 10, pp. 2073-2086,1991

7. R.D. Ferrante, M.J. Carlotto, P.W. Baim, and R.A. Upton, "Multi-spectral image analysis system," *First Conference on Artificial Intelligence Applications*, Dec. 1984, Denver CO.

8. B.G. Lee, V.T. Tom, and M.J. Carlotto, "A signal-symbol approach to change detection," Proceedings American Association of Artificial Intelligence, Philadelphia, PA., Aug. 1986.

9. Mark J. Carlotto and Michael C. Stein, "Detecting manmade changes in imagery," *Proceedings SPIE/Robotics*, Cambridge, MA, Nov. 1988.

10. "Welcome to Hell," *ABC News 20/20*, Show #1016, April 20, 1990, Journal Graphics, NY

11. L. A. Bartolucci and M. Chang, "Lookup tables to convert Landsat TM thermal IR data to water surface temperatures," *Geocarto International*, No.3, pp 61-67, 1988.

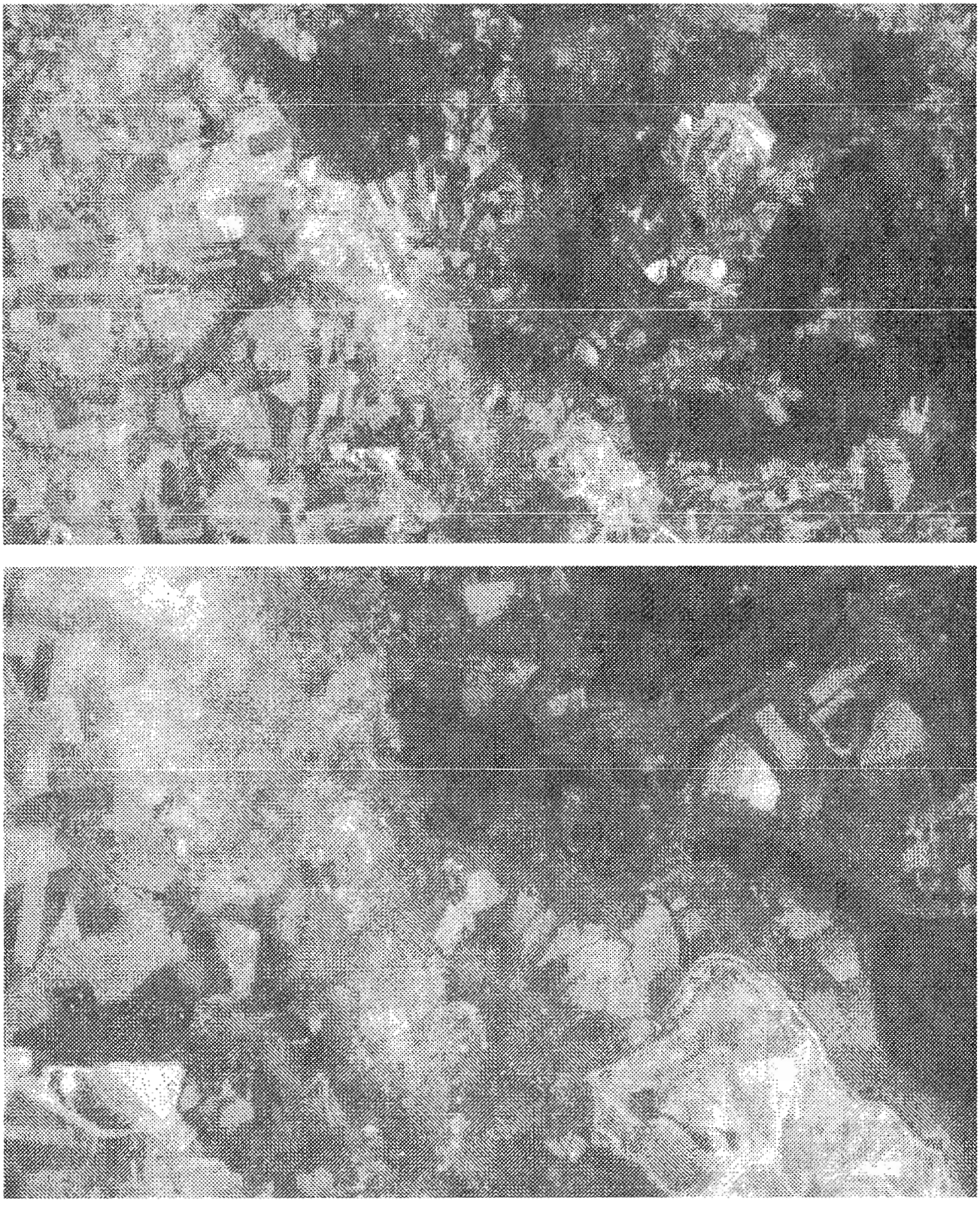

Fig. 7 Landsat TM imagery over Bitterfeld study area (top). Smoke plume originating from the city of Bitterfeld (bottom).

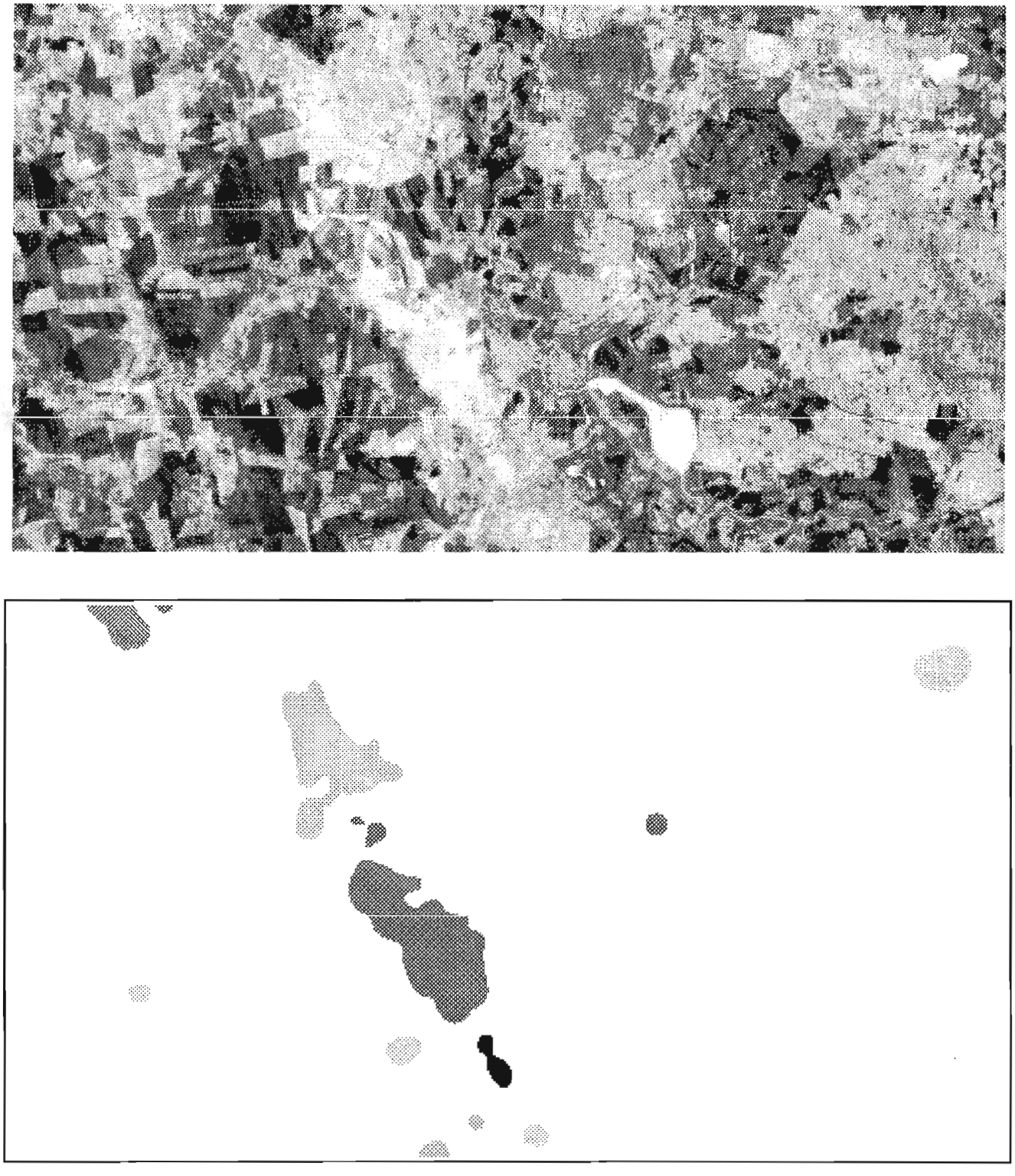

Fig. 8 TC4 image over Bitterfeld (top). Smoke plumes (darker areas) are regions that are relatively warm (bottom).

Fig. 9 Region-averaged MSVI shows forest damage north of Bitterfeld (dark areas).

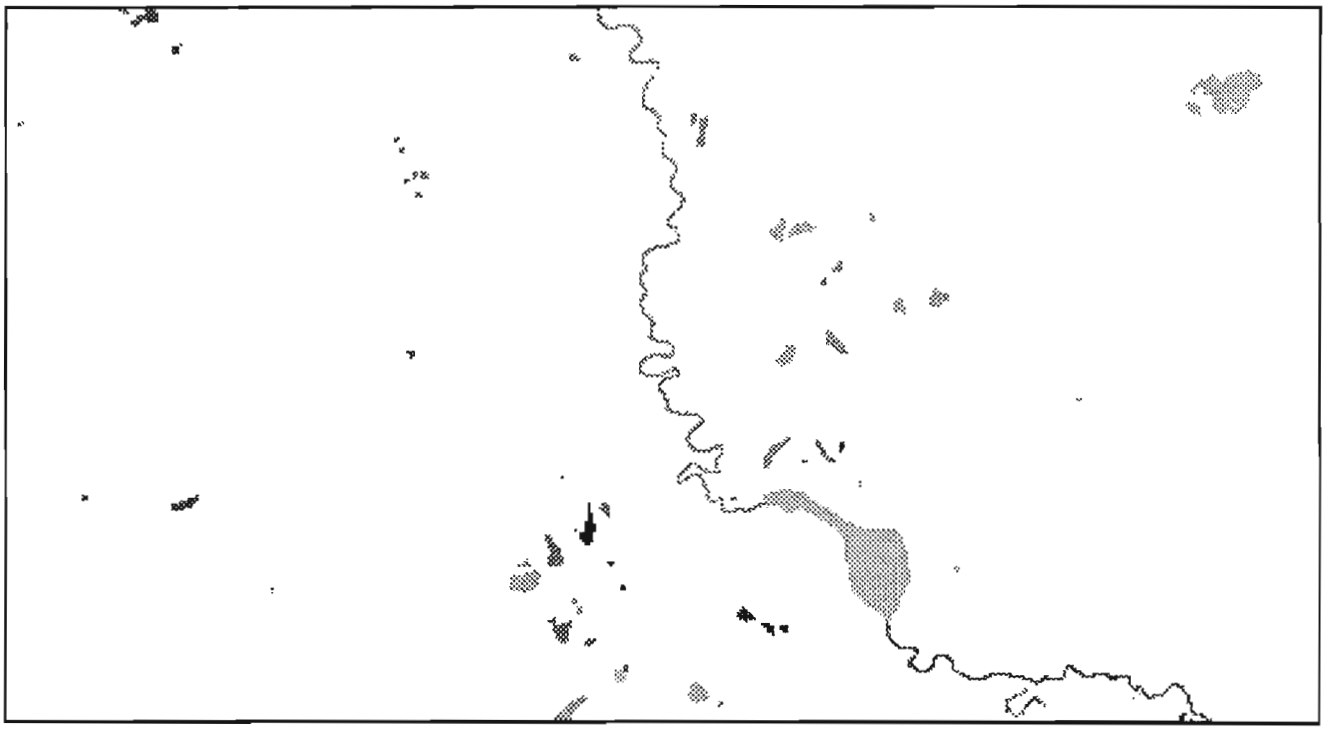

Fig. 10 Map of average water temperatures computed from thermal IR band. Relatively warm water is dark.

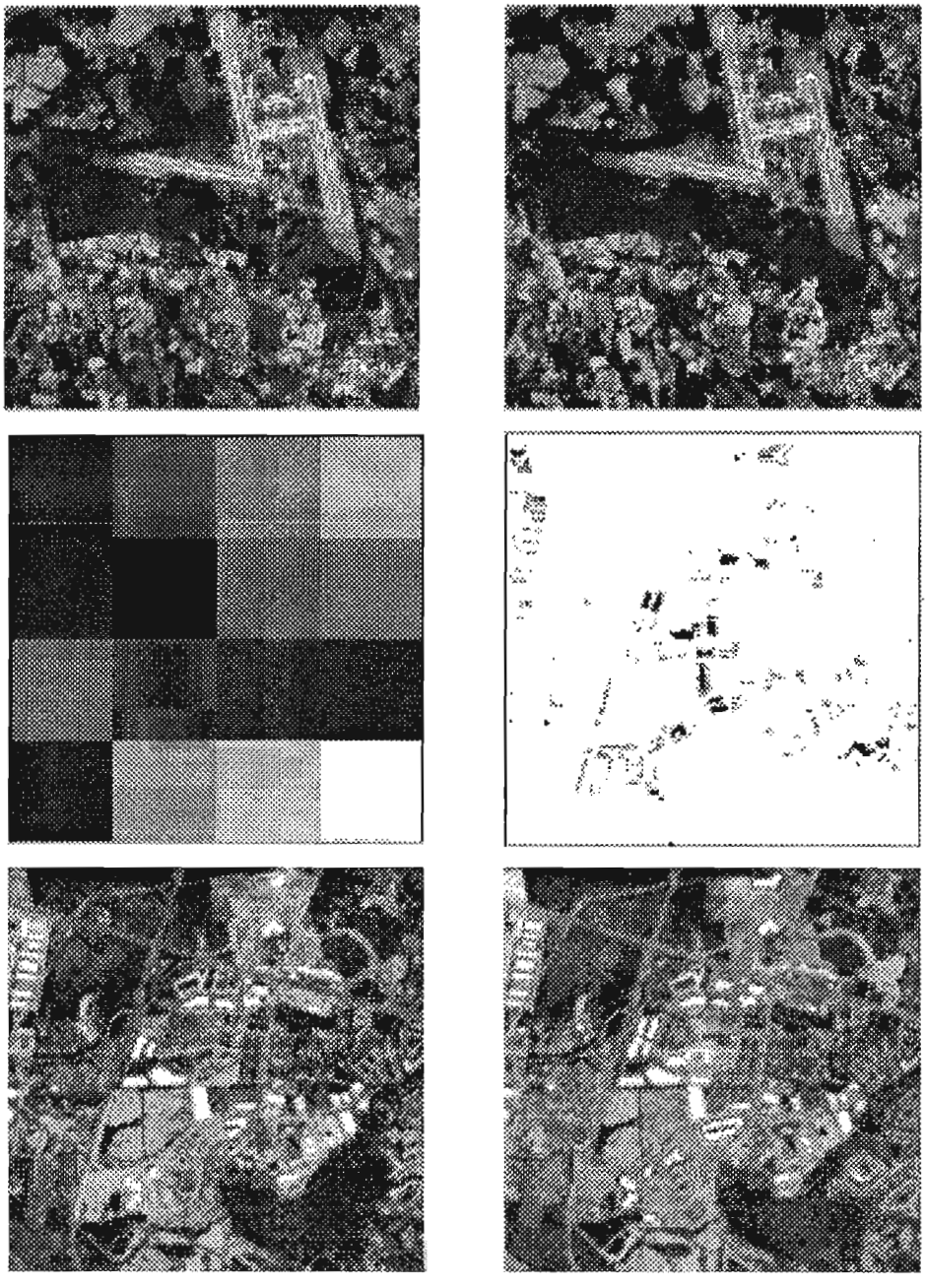

Fig. 11 Change detection results. 1024 by 1024 pixel images from SPOT over suburban Virginia acquired in 1987 (top left) and 1988 (top right). Average PCI computed over 256 by 256 sub-blocks (middle left). Corresponding SPOT data at full resolution from 1987 (bottom left) and 1988 (bottom right). Forward and backward prediction errors indicate possible appearances and disappearances in dark and midtones respectively (middle right).